OBSERVATIONS OF A SUPERCELL AND WEAK TORNADO MADE WITH A RAPID-SCAN, POLARIMETRIC, MOBILE RADAR

Alex Lyakhov [1,2], David Bodine[3,4], and Robert Palmer[3,4]

[1]2011 National Weather Center Research Experience for Undergraduates, Norman, Oklahoma
and
[2]State University of New York College at Oneonta, Oneonta, New York

[3]Atmospheric Radar Research Center, Norman, Oklahoma

[4]School of Meteorology, University of Oklahoma, Norman, Oklahoma

ABSTRACT

A rapid-scan, X-band, polarimetric, mobile Doppler radar is used to collect horizontal reflectivity, differential reflectivity, cross correlation coefficient and radial velocity data of a supercell that produced two EF-0 tornadoes in Osage County, OK on 18 June 2011. Volume scans of the first tornado, which lasted a few minutes, were acquired every 30 s. Analysis of data reveals several common polarimetric radar signatures associated with supercells including the low-level inflow, low-level hail and differential reflectivity arc signatures. The low-level inflow and differential reflectivity arc signatures both decreased in prominence around the time of tornado dissipation. No tornadic debris signature was noted, likely owing to the fact that the tornado was too weak to loft heavy debris, suggesting it is difficult for polarimetric radars to detect weak tornadoes. A Three Body Scatter Spike was also evident in the data, suggesting the presence of large hail aloft. Doppler velocity data reveal that mid-level mesocyclone intensification is not a pre-requisite for tornadogenesis. A trend of increasing azimuthal shear with time up to tornado dissipation is observed in the lowest two elevation scans, as well as within the low and midlevel mesocyclones. Azimuthal shear decreased after tornado dissipation in the lowest two scans and the low-level mesocyclone, but not with the midlevel mesocyclone. Furthermore, an anticyclonic circulation accompanied the cyclonic mesocyclone. A hook signature in the reflectivity field was observed with the mesoanticyclone, which later morphed into a linear feature.

1. INTRODUCTION

Supercell thunderstorms have been extensively studied by mobile radars due to the mobile radar's ability to navigate close to the storm and acquire high-resolution imagery. Polarimetric mobile radars are capable of distinguishing between hydrometeor types as well as between hydrometeors and tornadic debris (Ryzhkov et al. 2005). Numerous observational studies of supercells using polarimetric radars have been conducted (e.g., Loney et al. 2002; Ryzhkov et al. 2005; Heinselman and Ryzhkov, 2006; Bluestein et al. 2007; Van den Broeke et al. 2008; Kumjian and Ryzhkov, 2008; Kumjian and Ryzhkov, 2009; Kumjian et al. 2010; Palmer et al. 2010). Kumjian and Ryzhkov (2008) identified seven common polarimetric signatures associated with supercells such as the tornadic debris signature (TDS), hail signature in the forward-flank downdraft (FFD), low-level inflow/updraft signature, differential reflectivity (Z_{DR}) arc signature, Z_{DR} columns, specific differential phase (K_{DP}) columns, and midlevel Z_{DR} and cross correlation coefficient (ρ_{hv}) rings. Not every supercell will have every signature to the same extent. With rapid-scan polarimetric mobile radars, the ability to distinguish hydrometeors from non-meteorological targets is coupled with the ability to achieve volume scans in as low as 30 s at close proximity to supercells and tornadoes. This particular attribute is essential when trying to analyze the rapidly evolving, small-scale structures within supercells. It has been observed that only tens of seconds are needed for microscale structures such as tornadoes to alter their structure significantly **(**Bluestein et al. 2003**)**. Rapid-

Corresponding author address: Alex Lyakhov, 1632 East 18 Str., Apt. D11, Brooklyn, NY 11229.
E-mail: LYAKA87@suny.oneonta.edu

scan technology can be used to study the rapid evolution of particular polarimetric signatures in order to see how they correlate with the intensification of the mesocyclone or tornado.

The University of Oklahoma's School of Meteorology acquired a rapid-scan, X Band, polarimetric mobile radar in early 2011. The radar is known as the "RaXPol" and has already begun field operations. This radar was used to confirm the EF-5 strength of the tornado that struck El Reno, OK during the 24 May 2011 outbreak. On 18 June 2011, the RaXPol successfully acquired scans of a tornadic supercell in Osage County in northeastern Oklahoma. The tornado was rated EF-0 by the Tulsa, Oklahoma National Weather Service (NWS) office because the tornado touched down in a heavily wooded area and produced minimal tree damage. It touched down around 0109 UTC on 19 June 2011 and lifted a few minutes later. Volume scans during tornadogenesis, the tornado's mature stage and dissipation were completed every 30 s.

The following sections will provide information on the radar and data collected, the synoptic setup of the event, the polarimetric signatures associated with the supercell, the Doppler velocities associated with the tornadic and mesocyclonic circulations, and the anticyclonic circulation discovered in the data.

There are few rapid-scan observations of weak, brief tornadoes. The short duration of such tornadoes requires rapid-scan observations to adequately sample these rapid changes. This paper should provide insight on signatures associated with such tornadoes, which can then be compared with signatures associated with null tornado cases, funnel clouds, and violent tornadoes.

2. RADAR SPECS AND DATA COLLECTED

The RaXPol's ability to achieve scans with high temporal resolution makes that its most outstanding quality. This gives researchers the ability to sample the rapidly evolving nature of the tornado vortex and mesocyclone within the storm, particularly leading up to tornadogenesis.

The RaXPol was constructed by ProSensing Inc. and made available to the University of Oklahoma (OU) when OU purchased it for $1.25 million. The antenna diameter is 2.4 m, yielding a beamwidth of 1.1°. The polarization is dual linear (vertical and horizontal) and gain of the antenna is 44 dBi. The radar has a wavelength of 3 cm (X-band). The pulse repetition frequency (PRF) can be as high as 5 kHz and is staggered to reduce velocity ambiguities. The operating frequency range of the radar is 9.7-9.8 GHz. The transmitter is a CPI air-cooled X-band Coupled Cavity Travelling Wave Tube Amplifier with 20 kW of minimum peak power.

RaXPol's high temporal resolution is achieved by having the maximum speed of the pedestal be 180° s^{-1} azimuth and 20° s^{-1} elevation. Therefore, assuming 10 elevations are the desirable number of elevations to be scanned, the RaXPol can complete an entire volume scan in 20 s. Given this rapid-scan capability and lowered dwell-time, sensitivity can be expected to decrease. According to ProSensing, the sensitivity during rapid-scan mode is -16 dBZ at 30 km. Also, a maximum unambiguous velocity of 31 ms^{-1} means that weak tornadoes can be sampled without dealing with cumbersome aliased velocity data. Velocities sampled over 31 ms^{-1} will have to be unfolded in order to determine the true velocity. Attenuation is another potential issue facing the RaXPol. Radars that operate in X-band are known to have attenuation issues. Therefore, any research done in which a tornado is to be sampled should have the radar scan the storm with minimal precipitation between the radar and the tornado to prevent severe attenuation near the tornado.

The dataset includes data on a supercell that reportedly produced 2 tornadoes. According to the Tulsa, Oklahoma NWS office, the first tornado (Tornado 1) touched down at 0109 UTC approximately 7 mi NNW of Bigheart, Oklahoma. Visibility was reduced from the radar's perspective as a result of precipitation between the radar and tornado, so we cannot confirm exactly what time the tornado touched down. It is possible that the tornado touched down a few minutes earlier and was not reported until 0109 UTC; however, this cannot be proven. A case is made for the tornado potentially touching down at 0105:30 UTC in Section 5.2. The second tornado (Tornado 2) touched down a few minutes after Tornado 1 lifted.

This particular report came to the SPC at 0125 UTC with the wording "several storms chasers ... storm spotters and at least one off duty National Weather Service meteorologist witnessed this tornado. It lasted 10 to 15 minutes and produced no known damage." The exact time of Tornado 1 dissipation and Tornado 2 formation is not known to the authors, once again, due to low visibility and the author's distance from the tornado.

In the case presented herein, the RaXPol was located approximately 20 km east of Tornado 1 during data collection. The tornado was observed reasonably well, however, significant attenuation is apparent on the opposite (western) side of the hail/precipitation core (Figure 9). The radar performed volume scans with 13 elevations with the 0.8° elevation scan being the lowest and 13° the highest.

3. STORM ENVIRONMENT

The supercell formed within an environment with convective available potential energy (CAPE) values around 3500 J kg^{-1} and storm relative environmental helicity (SREH) values around 155 $m^2 s^{-2}$, according to the proximity sounding taken at 0000 UTC 19 June 2011 in Springfield, Missouri (Figure 1). The surface plot in Figure 2 indicates that conditions were favorable for severe storm development in northeastern Oklahoma and southeastern Kansas due to sufficiently warm temperatures (around 90°F) and high dewpoints (70-75°F). A stationary front was present from east central Kansas to south central Kansas with a cold front extending into west central Oklahoma (not shown). The boundary associated with the stationary front provided adequate surface forcing for severe storms to develop.

The 0000 UTC 850 hPa analysis (Figure 3) shows that temperatures are between 20 and 30°C with dewpoints between 10 and 20°C in the region where the supercell developed. Warm air advection is evident across Oklahoma into southwestern Missouri. A shortwave trough is visible in the 500 hPa vorticity and wind analysis (Figures 4 and 5 respectively) stretching from north to south from western South Dakota to north central Texas. The 300 hPa analysis reveals a lack of any substantial jet streams overhead (not shown), although winds at this level were still 50-60 kts as shown by the sounding. The presence of a 500 hPa shortwave trough and 850 hPa warm air advection acted to enhance synoptic scale lift, potentially providing additional support for severe storm development.

Storms formed around 2300 UTC along the Kansas and Oklahoma border and progressed eastward. The supercell discussed in this paper formed near Arkansas City, Kansas and proceeded to traverse east southeastward, nearly parallel to the Kansas and Oklahoma border.

4. POLARIMETRIC RADAR SIGNATURES

Common polarimetric radar signatures of supercells were documented by Kumjian and Ryzhkov (2008). These signatures are found by analyzing the values of variables such as horizontal reflectivity (Z), Z_{DR}, ρ_{hv} and K_{DP}. A few of the common polarimetric radar signatures were documented with this supercell including the low-level inflow signature, the low-level hail signature, and the Z_{DR} arc. No clear tornadic debris signature (TDS) was documented; potential reasons for this will be discussed in this section.

4.1 *Low-level inflow signature*

Strong low-level inflow was evident during the mature stage of the supercell. A "tongue" of lower ρ_{hv} values are seen wrapping around the mesocyclone from east of the circulation to the northwestern flank of the circulation. These lowered ρ_{hv} values are collocated with lowered Z values. The low Z values wrapping around the mesocyclone are a feature of a Bounded Weak Echo Region (BWER). Given Z values in the 12-22 dBZ range collocated with ρ_{hv} values in the 0.65-0.75 range, such as in Figure 6, it can be reasonably assumed that inflow winds were picking up irregularly shaped nonmeteorological scatterers such as dirt, leaves, bugs and grass and lifting them high enough to be detected by radar. Precipitation particles may have been mixed in as well (Kumjian and Ryzhkov, 2008). This image was taken at approximately the time of tornadogenesis. By 0110:30 UTC, the low-level inflow signature is not as prominent given ρ_{hv} values not wrapping as far around the mesocyclone (Figure 7). This may be a result of weaker winds picking up fewer nonmeteorological scatterers or more precipitation falling as a result of a weaker updraft.

4.2 *Low-level hail signature*

Severe hail (larger than or equal to 1 inch in diameter) was reported with this storm (see SPC storm reports website). The largest hail diameter reported was 2.5 in, 3.2 km ENE of Maple City, KS at 2342 UTC. Unfortunately, the radar was in transit during this time.

A polarimetric Three-Body Scatter Spike (TBSS) is observed, characterized by the presence of an area of low Z (0-10 dBZ), high Z_{DR} (6-8 dB) and very low ρ_{hv} (0.1-0.3) values a few km to the northwest of the mesocyclone. Figure 8 shows the Z, Z_{DR} and ρ_{hv} values at 3.9° tilt at 0104:30 UTC. With the area most likely to contain hail being located between the radar and the TBSS in the 0104:30 UTC scans, it can be assumed that hailstones present within the radar beam caused such a signature. Previous research on the TBSS concluded that it is caused by Mie-scattering from an area containing a large concentration of large hydrometeors (Lemon, 1998) and by multiple scattering between hydrometeors and the ground (Zrnić, 1987). Lemon (1998) also came to the conclusion that the presence of a TBSS preceded surface hail fall, and can therefore be used by forecasters to assess the likelihood of hail falling with a particular storm.

The 0107 UTC scan (Figure 9) at the same elevation reveals an area of anomalously depressed Z and Z_{DR} values oriented east-west stretching for approximately 10 km to the north of the mesocyclone. This is likely due to attenuation as a result of the presence of a hail core. Hail, large raindrops, or a combination of both to the north and northeast of the mesocyclone is implied given the presence of high Z and relatively lower ρ_{hv} values (45-60 dBZ and 0.75-0.90 respectively) where there is no attenuation. Attenuation makes determining the true Z_{DR} value where hail likely exists difficult. However, high Z_{DR} is seen to the east of the area of attenuation. Therefore, it is reasonable to assume Z_{DR} is in fact high despite the attenuation making it seem as though it were lower. The size of these hailstones is theorized to be smaller than 1.5-2.0 cm. Hail of this size often obtains a water shell (Rasmussen et al. 1984). The presence of water on the surface of the hailstone tends to reduce the chaotic nature of its orientation, thus increasing Z_{DR}. When scanned by radar, small, wet hailstones appear as large raindrops with high Z_{DR} values (Kumjian and Ryzhkov, 2008). However, Kumjian and Ryzhkov (2008) mention that the effects of intense attenuation and resonance scattering at shorter wavelengths means that radar measurements at C-band require special considerations. Such considerations should be applied to radar measurements at X-band, such as in this case. There may well be large hail present downstream of the mesocyclone despite high Z_{DR} readings. The combination of very large raindrops, large, dry hail and melting hailstones can produce high Z_{DR}. Therefore, it is impossible to know with a high degree of certainty whether or not very large hail existed with this supercell at this time by only looking at the radar data. Nevertheless, SPC storm reports indicate that pea to quarter sized hail was falling during the time these scans were taken.

4.3 *Z_{DR} arc*

The Z_{DR} arc is typically found along the southern edge of the forward-flank downdraft (FFD) where locally higher Z_{DR} values form an "arc" shape. Size sorting of particles by the updraft plays a key role in forming the arc. These high Z_{DR} values are primarily associated with very large, oblate raindrops. Z_{DR} drops off with increasing distance from the updraft. Intuitively, the largest particles will exist close to the updraft and will fall to the ground close to the updraft while smaller particles will be able to stay suspended for a longer period of time and can therefore be carried further downstream of the updraft. Moreover, Kumjian and Ryzhkov (2009) show that the Z_{DR} arc can serve as a proxy for low-level storm-relative environmental helicity (SREH; Davies-Jones et al. 1990). A stronger Z_{DR} arc implies that horizontal vorticity is being ingested by the updraft, which may precede the development of a tornado (Kumjian and Ryzhkov, 2008).

The 0058:24 UTC 3° elevation scan (Figure 10) reveals a striking Z_{DR} arc characterized by Z_{DR} values in the 5-7 dB range. Z_{DR} was this high for a few more scans before being primarily in the 4-5 dB range through the majority of the supercell's mature stage. However, from 0108-0111 UTC, the Z_{DR} arc can be seen decreasing in prominence and a region of lower Z_{DR} values develops within the arc (Figure 11). This suggests a reduction in the amount of horizontal

vorticity being ingested by the updraft, which can lead to a weakening tornadic circulation. Doppler velocity data did indeed depict a weakening tornadic circulation at the same time, which will be discussed in Section 5.2.

4.4 *Tornadic debris signature*

Tornadic debris signatures (TDS) are characterized by anomalously low ρ_{hv} values along with low Z_{DR} and high Z values within the hook of the storm. The random orientation and irregular shape of most debris lofted by tornadoes causes ρ_{hv} to be lowered. The chaotically tumbling nature of large debris would cause Z_{DR} to decrease while the presence of many small or a few large pieces of debris would cause high Z values. Previous research on the detection of tornadoes using polarimetric radar has postulated that the tornado has to be at least F3 strength in order for a TDS to persist for multiple scans. It was also found that most weak tornadoes did not produce a TDS likely owing to the fact that their winds are too weak to cause or lift debris or that they are too short lived, which would cause radars with poor temporal resolution to miss the debris all together (Ryzhkov et al. 2005b). However, Kumjian and Ryzhkov (2008) mention that KOUN detected a TDS with an EF-1 tornado on 9 May 2007.

In the case presented here, no clear TDS was documented most likely due to the tornado's weak (EF-0) winds. Interestingly, the 2° scan at 0109 UTC (approximately the time of tornado touchdown) shows reduced ρ_{hv} (0.75-0.85) near the circulation (Figure 12), which may indicate some light debris being lofted. It is unlikely that there was any large debris lofted by the tornado. Its touchdown location was likely not a major reason for the lack of a TDS because heavily wooded areas should still have the ability to provide sufficient debris to produce a TDS. However, if the winds are too weak to break off enough branches and suspend them in the air, no TDS can be expected to form. Other possible reasons for a lack of a TDS include the radar being too far away, so radar beams may have been scanning above the level where the debris was located. In addition, the signal from precipitation may have been stronger than the signal from the small amount of debris lofted, which would obscure the debris signal.

5. DOPPLER VELOCITIES and AZIMUTHAL SHEAR

This section will analyze the Doppler velocities and azimuthal shear associated with the low and midlevel mesocyclones prior to, during, and after tornadogenesis. Specifically, the time leading up to tornadogenesis and the time following tornado dissipation will be examined. Velocities of the tornadic circulation will be analyzed as well. As a reminder, only the first tornado spawned by the supercell (Tornado 1) will be analyzed. Given that the radar was approximately 20 km away from the tornado at its closest, high enough resolution data are not available to adequately sample the tornado itself. However, the tornadic circulation was observable by radar with the caveat of velocities measured within the gates being highly averaged. Topics to be addressed include how the strength of the shear within the low-level and midlevel mesocyclones changed (if at all) prior to, during, and after tornadogenesis. In addition, the strength of the gate-to-gate shear associated with the EF-0 tornado will be examined.

5.1 *Mid and low-level mesocyclone*

Figure 13 illustrates the change in azimuthal shear with time of the midlevel and low-level mesocyclones. The elevation angles that were determined to have sampled the mid and low-level mesocyclones are the 9.9° and 3.9° elevation angles (respectively). The distance above ground of the midlevel mesocyclone sampled by the 9.9° scan is approximately 3.4 km. Meanwhile, the distance above ground of the low-level mesocyclone sampled by the 3.9° scan is approximately 1.45 km. Shear with the midlevel mesocyclone generally remained between .0012 and .0019 s^{-1}.

Meanwhile, azimuthal shear with the low-level mesocyclone varied between .0009 and .0016 s^{-1}. Values appear to show an increasing trend leading up to tornadogenesis (prior to 0109 UTC) and a decreasing trend after tornado dissipation (around 0109 UTC). Unlike in the low-level mesocyclone, azimuthal shear after tornado dissipation *increases* with the midlevel mesocyclone. Therefore, we cannot conclude that midlevel mesocyclone weakening is required for tornado dissipation.

Additionally, Figure 14 shows the change of the circulation diameter with time. Both the mid and low-level mesocyclones appear to contract their circulations after 0107 and 0106:30 UTC, respectively. Notably, the low-level mesocyclonic circulation contracts from about 4 km at 0106:30 UTC to about 2 km at 0109 UTC, followed by an expansion to about 3 km thirty seconds later. Angular momentum considerations associated with tornadogenesis at the surface are likely relevant in this case.

It is worth noting that the 8.9° scan shows a distinct increase in azimuthal shear between 0107 and 0109 UTC (not shown). Maximum azimuthal shear was recorded at .0058 s^{-1} at 0109 UTC before dropping to .0025 s^{-1} in the following scan thirty seconds later. Potential reasoning for this is that a tornado vortex signature (TVS) was noted in the 8.9° scan at 0109 UTC (Figure 15). A TVS was also present at the 0.8° scan at the same time (Figure 16), and was observed in radial velocity from 0.358 km to 3.175 km above ground (0.8° to 8.9°, respectively) (not shown), which is the maximum height of the circulation. This would account for the seemingly anomalous spike in azimuthal shear.

5.2 *Tornado*

Although ground confirmation of touchdown time is unavailable, the tornado may have been on the ground as early as 0105:30 UTC given the maximized gate-to-gate velocities in Figure 17. Nonetheless, it may just have been the funnel cloud that was being sampled.

The 0.8° and 1.9° elevation angles were utilized to determine the azimuthal shear associated with the tornadic circulation near the surface. Height above ground of the radar beams sampling the tornado is approximately 350 m with the 0.8° elevation scan and 750 m with the 1.9° scan. Figure 18 shows a general trend of increasing shear values with time. Maximum shear values were recorded at 0108:30 UTC and 0109 UTC with the 1.9° and 0.8° scans (respectively). This peak value that was recorded is approximately .0041 s^{-1} for both elevation angles. Figure 16 shows the velocity field in the 0.8° scan at 0109 UTC. This is when the strongest gate-to-gate velocities were measured at this elevation: 31 ms^{-1}. A notable decline in shear is evident in both elevation scans at 0109:30 UTC. Thus, it is reasonable to assume that the tornado dissipated between 0109 and 0109:30 UTC, which was corroborated by visible observations of the funnel becoming more poorly defined. Such a rapid weakening indicates that rapid-scan observations are needed to understand tornado dissipation.

6. MESOANTICYCLONE

The 1.9° elevation scan at 0101:30 UTC reveals an appendage structure in the reflectivity extending southward from the hook echo (Figure 19a). Velocity data reveal the presence of relatively strong (~25 ms^{-1}) inbound winds likely associated the rear-flank gust front surge a few km west of this appendage (Figure 19b). By 0105 UTC, an anticyclonic circulation is visible in the velocity data collocated with the beginnings of what will later become the anticyclonic hook (Figure 20). This anticyclonic hook is more prominent in the 3° scan at 0106:30 UTC (Figure 21). The circulation associated with the mesoanticyclone is noticeably weaker than that of the tornadic circulation approximately 5 km to the NNW. At 0108:30 UTC, the reflectivity field shows the 1-km wide band of higher reflectivities (30-40 dBZ) wrapping around the western side of the mesoanticyclone (Figure 22), and by 0109:30 UTC, the hook signature is no longer well-defined (Figure 23). The mesoanticyclone later weakens probably due to influences of occlusion of the updraft. A linear feature associated with the mesoanticyclone is noted in reflectivity. This linear feature is more prominent at 0111 UTC (Figure 24).

7. SUMMARY

Successful scans of a supercell and associated weak (EF-0) tornado were made on 18 June 2011 with a rapid-scan, polarimetric, X-band mobile radar known as the RaXPol. Common polarimetric signatures associated with supercells were noted with the storm including the low-level inflow signature, low-level hail signature and the Z_{DR} arc.

The low-level inflow signature is characterized by a narrow band of low ρ_{hv} and Z values wrapping around the mesocyclone. This occurs when nonmeteorological scatterers such as leaves, dirt and bugs are picked up and carried by the inflow winds. This signature became less prominent at approximately

the time of tornado dissipation, suggesting weakened inflow winds or more precipitation in the inflow region due to a weaker updraft. The low-level hail signature was characterized by attenuation as well as high Z and Z_{DR} and low ρ_{hv} values to the north and northeast of the mesocyclone. Pea to quarter size hail was indeed reported falling with the storm. In addition, a polarimetric TBSS was noted, caused by multiple scattering of the radar beams between hail and the ground. A Z_{DR} arc, in which a band of high Z_{DR} exists on the southern edge of the FFD, was seen. This can serve as a proxy for storm-relative environmental helicity. The Z_{DR} arc became less prominent at around the time of tornado dissipation. This may imply a decrease in the amount of horizontal vorticity ingested by the updraft, which can precede tornado dissipation. No clear TDS was identified, although slightly lowered ρ_{hv} values at 0109 UTC may indicate some light debris being lofted.

Trends of strengthening azimuthal shear before 0109 UTC (tornado dissipation) were documented at the levels where the tornado, low-level mesocyclone and midlevel mesocyclone existed. Shear at the two lowest tilts decreased dramatically after 0109 UTC, within only 30 – 60 s. Azimuthal shear within the low-level mesocyclone decreased by almost a factor of two after 0109 UTC. However, shear within the midlevel mesocyclone maintained its increasing trend. For that reason, it cannot be concluded that the weakening of the midlevel mesocyclone is a prerequisite for tornado dissipation. Furthermore, in addition to the cyclonic circulation associated with the tornado and mesocyclone, an anticyclonic circulation developed on the southern end of the supercell's hook, likely a result of the rear-flank gust front surge. It developed a few minutes prior to tornadogenesis (with the cyclonic circulation) and dissipated at about the same time as the dissipation of the tornado (0109 UTC).

The rapid-scan and dual-polarization capability of the RaXPol allowed the researchers to examine the rapidly evolving structures and get a sense of hydrometeor types and locations within the supercell. Additional research should be conducted on supercells that do not produce tornadoes, ones that only produce funnel clouds, and ones that produce violent tornadoes to compare their polarimetric signatures in the hopes that once the WSR-88D radar network acquires polarization capability; forecasters will be better able to distinguish among the different types of tornado events caused by supercells.

8. ACKNOWLEDGEMENTS

This paper was made possible thanks to Daphne LaDue and the Research Experience for Undergraduates (REU) Program. Additional thanks to Tim Bonin for helping with the radar during deployment. This work was prepared by the authors with funding provided by National Science Foundation Grant No. AGS-1062932. The funding for the RaXPol was provided by National Science Foundation Grant No. AGS-0821231. The statements, findings, conclusions, and recommendations are those of the authors and do not necessarily reflect the views of the National Science Foundation.

9. REFERENCES

Bluestein, H.B., M.M. French, R.L. Tanamachi, S. Frasier, K. Hardwick, F. Juyent, and A.L. Pazmany, 2007b: Close-range observations of tornadoes in supercells made with a dual-polarization, X-band, mobile, Doppler radar. *Mon. Wea. Rev.*, **135**, 1522-1543.

Davies-Jones, R., D.W. Burgess, and M. Foster, 1990: Test of helicity as a forecast parameter. Preprints, *16th Conf. on Severe Local Storms*, Kananaskis Park, Alberta, Amer. Meteor. Soc., 588-592.

Heinselman, P.L., and A.V. Ryzhkov, 2006: Validation of polarimetric hail detection. *Wea. Forecasting*, **21**, 839–850.

Kumjian, M.R. and A.V. Ryzhkov, 2008: Polarimetric signatures in supercell thunderstorms. *J. Appl. Meteor. and Climatology*,**48**,1940-1961.

Kumjian, M.R. and A.V. Ryzhkov, 2009: Storm-relative helicity revealed from polarimetric radar measurements. *J. Atmos. Sci.*, **66**, 667-685.

Lemon, L.R., 1998: The radar "Three-Body Scatter Spike": An operational large-hail signature. *Wea. Forecasting*, **13**, 327-340.

Loney, M.L., D.S. Zrnić, J.M. Straka, and A.V. Ryzhkov, 2002: Enhanced polarimetric radar signatures above the melting level in a

supercell storm. *J. Appl. Meteor*.,**41**, 1179-1194.

Palmer, R.D., D. Bodine, M. Kumjian, B. Cheong, G. Zhang, Q. Cao, H. Bluestein, A. Ryzhkov, T.-Y. Yu, Y. Wang, The 10 May 2010 Tornado Outbreak in Central Oklahoma: Potential for New Science with High-Resolution Polarimetric Radar, *Bull. Amer. Meteor. Soc.*, in press.

Rasmussen, R.M., V. Levizzani and H.R. Pruppacher, 1984: A wind tunnel and theoretical study on the melting behavior of atmospheric ice particles, III: Experiment and theory for spherical ice particles of radius ≥ 500 μm. *J. Atmos. Sci.*, **41,** 381-388.

Ryzhkov, A.V., T.J. Schuur, D.W. Burgess, and D.S. Zrnić, 2005b: Polarimetric tornado detection. *J. Appl. Meteor.*, **44**, 557–570.

Van Den Broeke, M. S., J. M. Straka, and E. N. Rasmussen, 2008: Polarimetric radar observations at low levels during tornado life cycles in a small sample of classic Southern Plains supercells. J. Appl. Meteor. Climatol., **47,** 1232–1247.

Zrnić, D.S., 1987: Three-body scattering produces precipitation signature of special diagnostic value. *Radio Sci.*, **22**, 76-86.

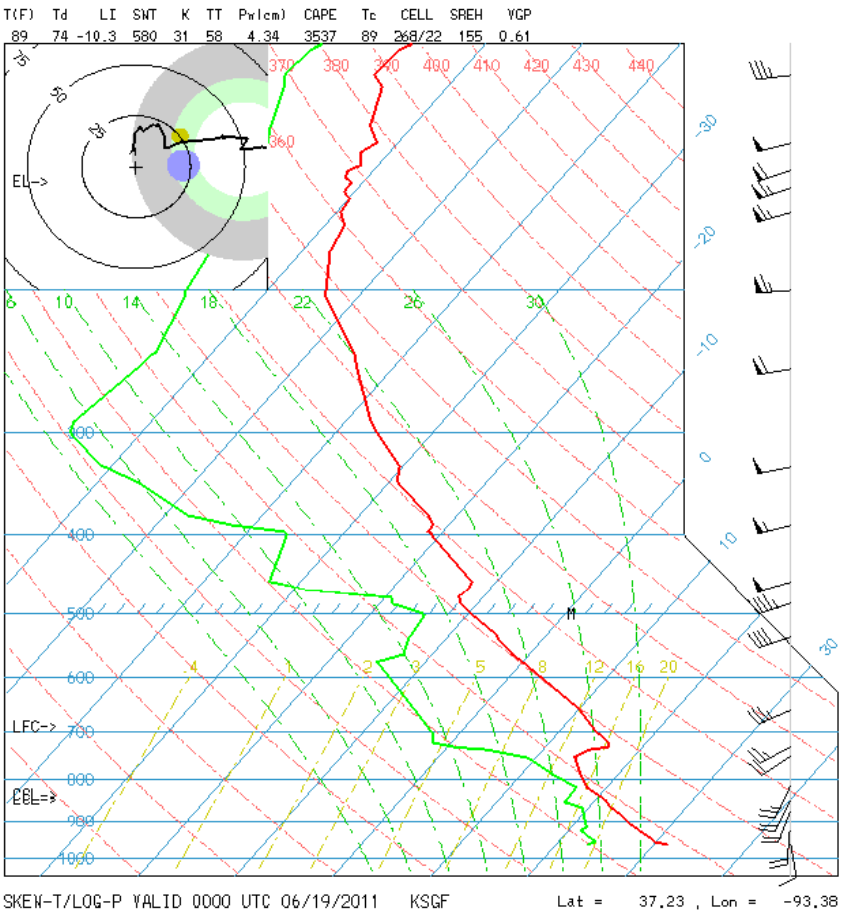

Figure 1: Springfield, Missouri (KSGF) sounding taken 0000 UTC on 19 June 2011.

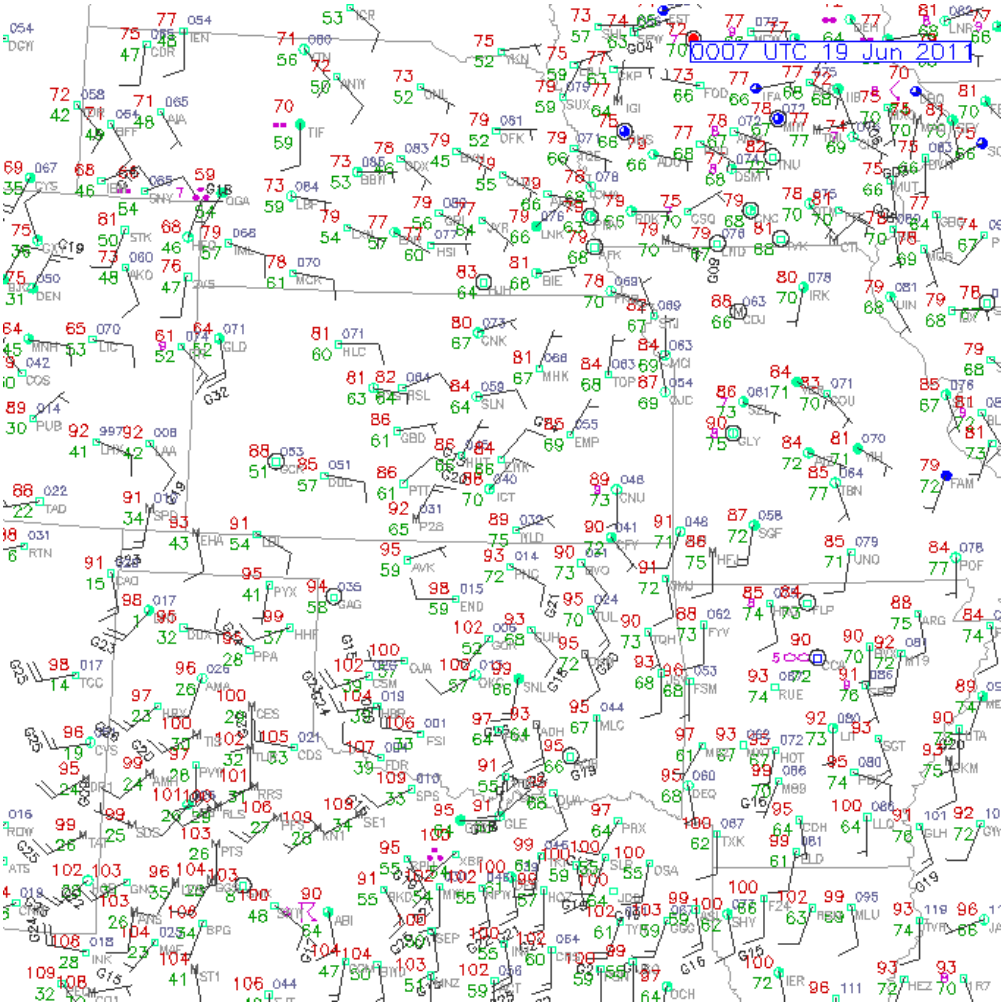

Figure 2: Station plots of the Central Plains taken at 0007 UTC on 19 June 2011.

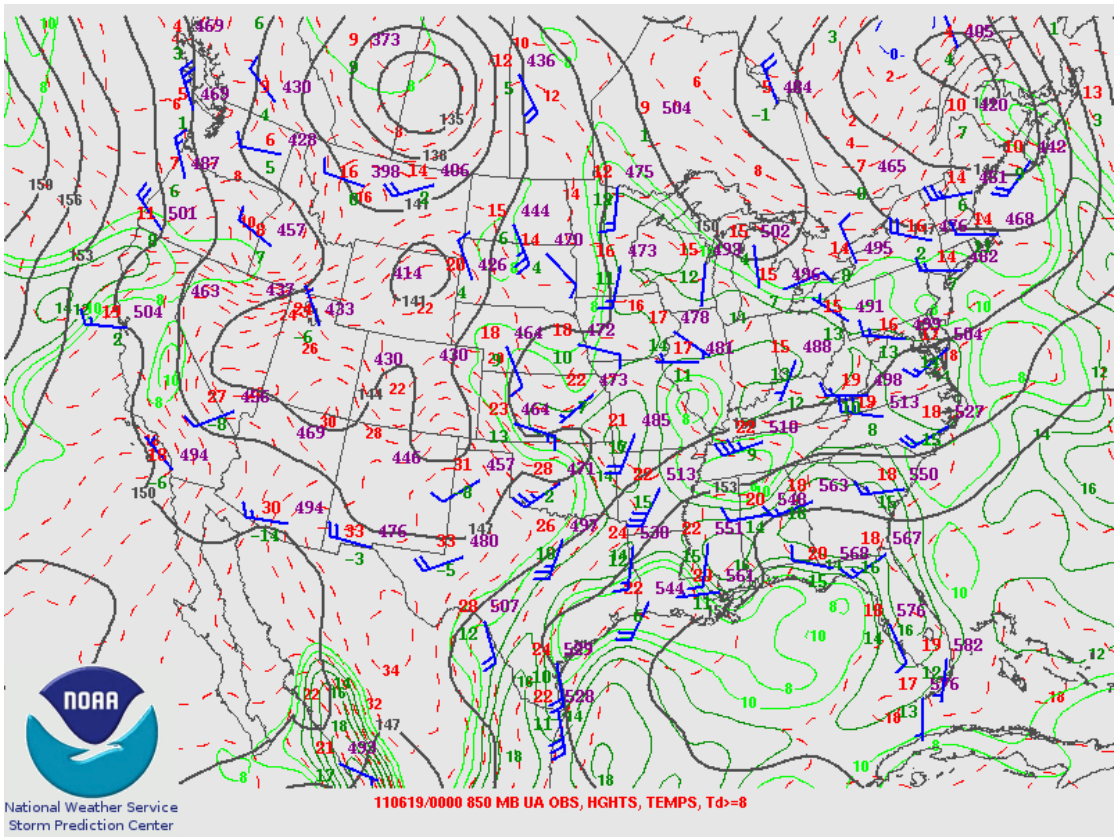

Figure 3: 850 hPa analysis at 0000 UTC on 19 June 2011.

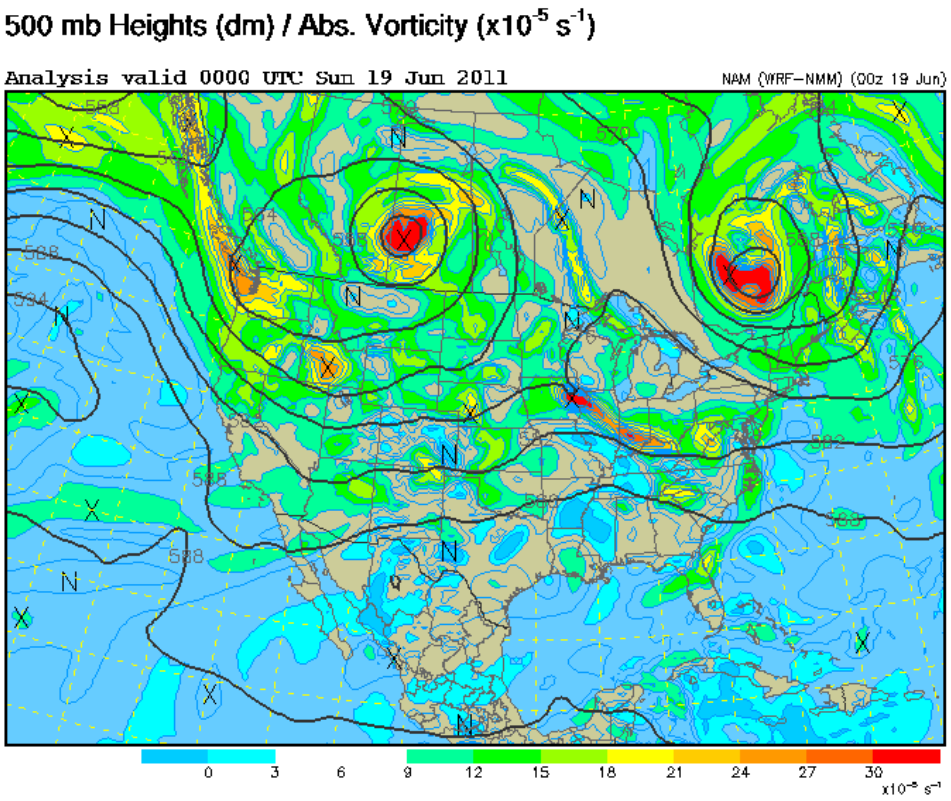

Figure 4: As in Figure 3, except for 500 hPa vorticity.

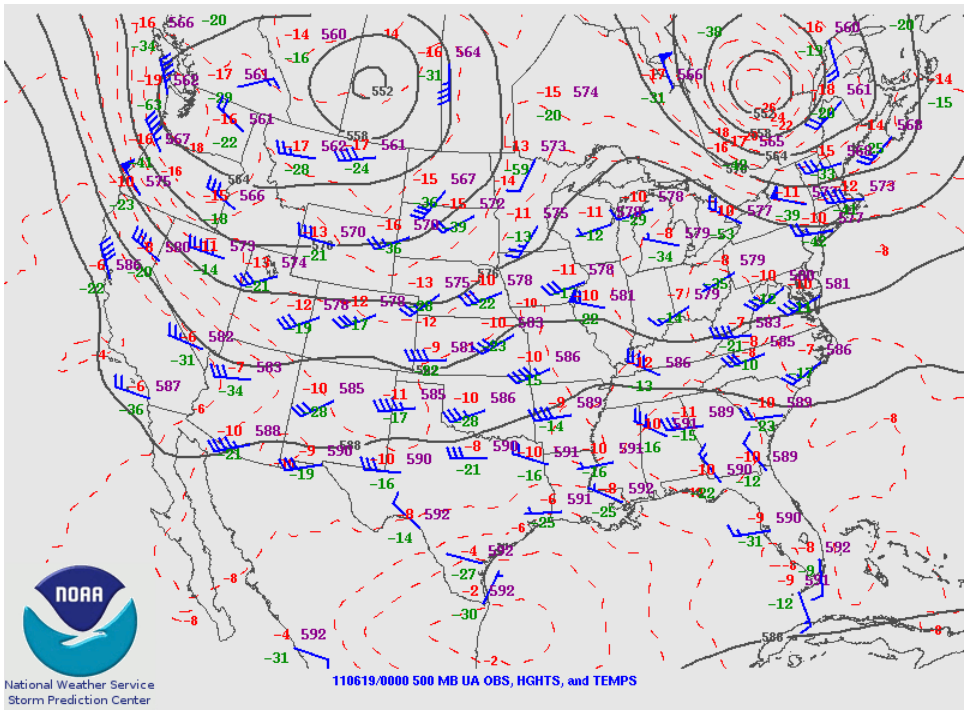

Figure 5: As in Figure 3, except for 500 hPa.

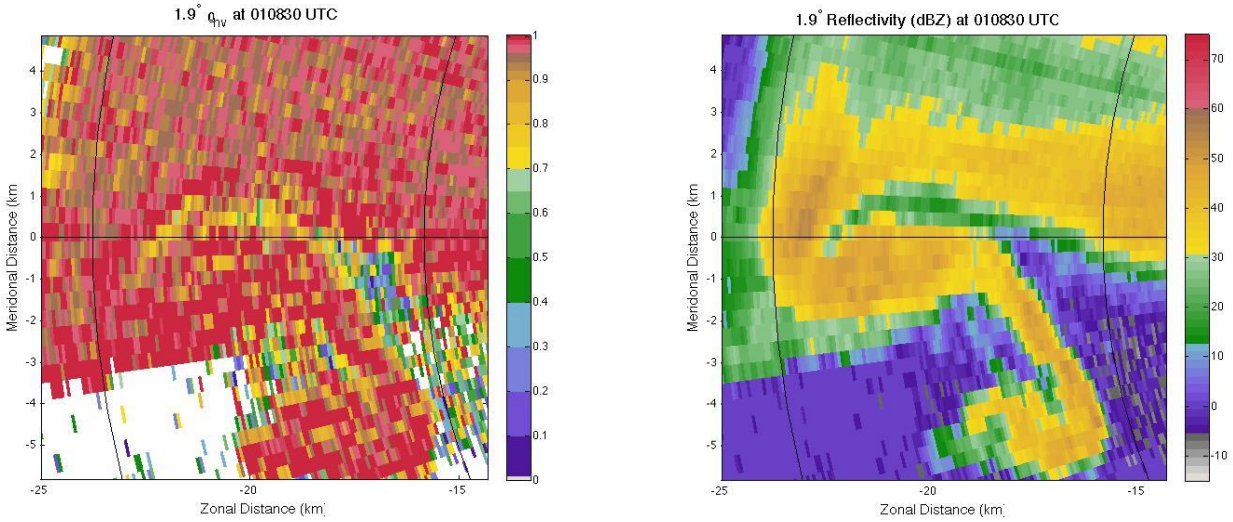

Figure 6: 1.9° elevation scan showing ρ_{hv} and Z at 0108:30 UTC.

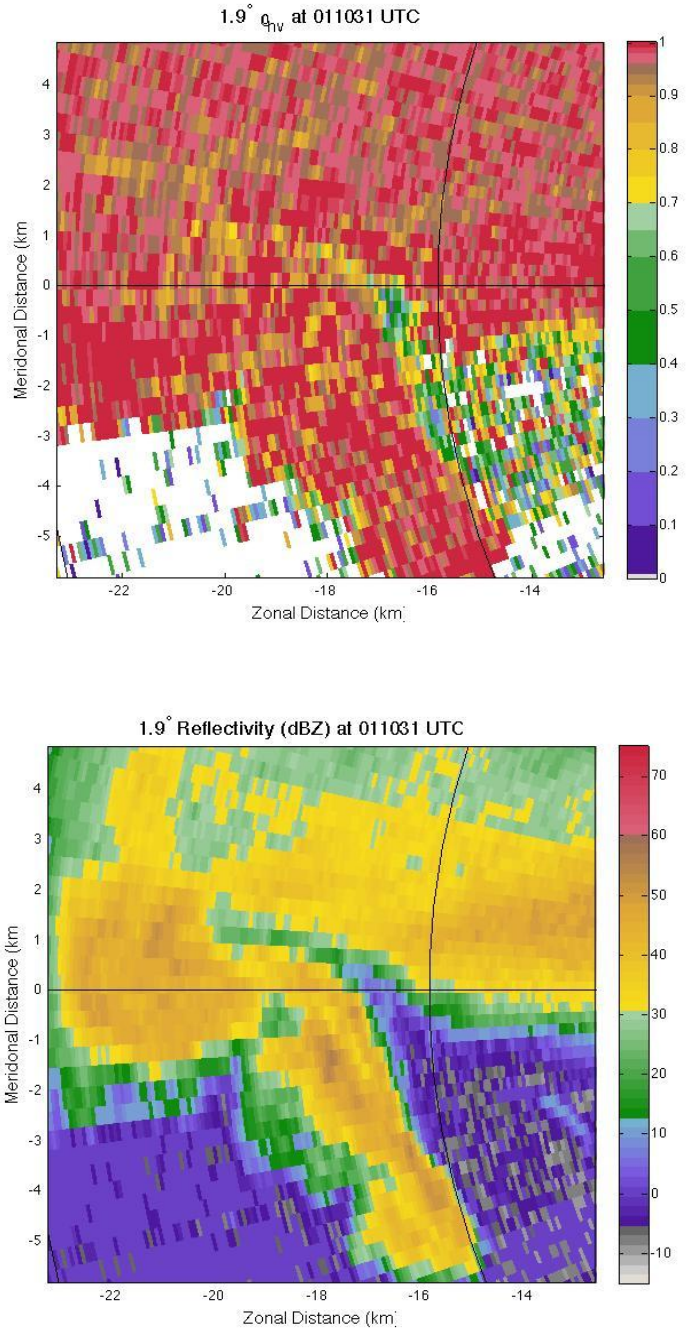

Figure 7: As in Figure 6, except for 0110:30 UTC.

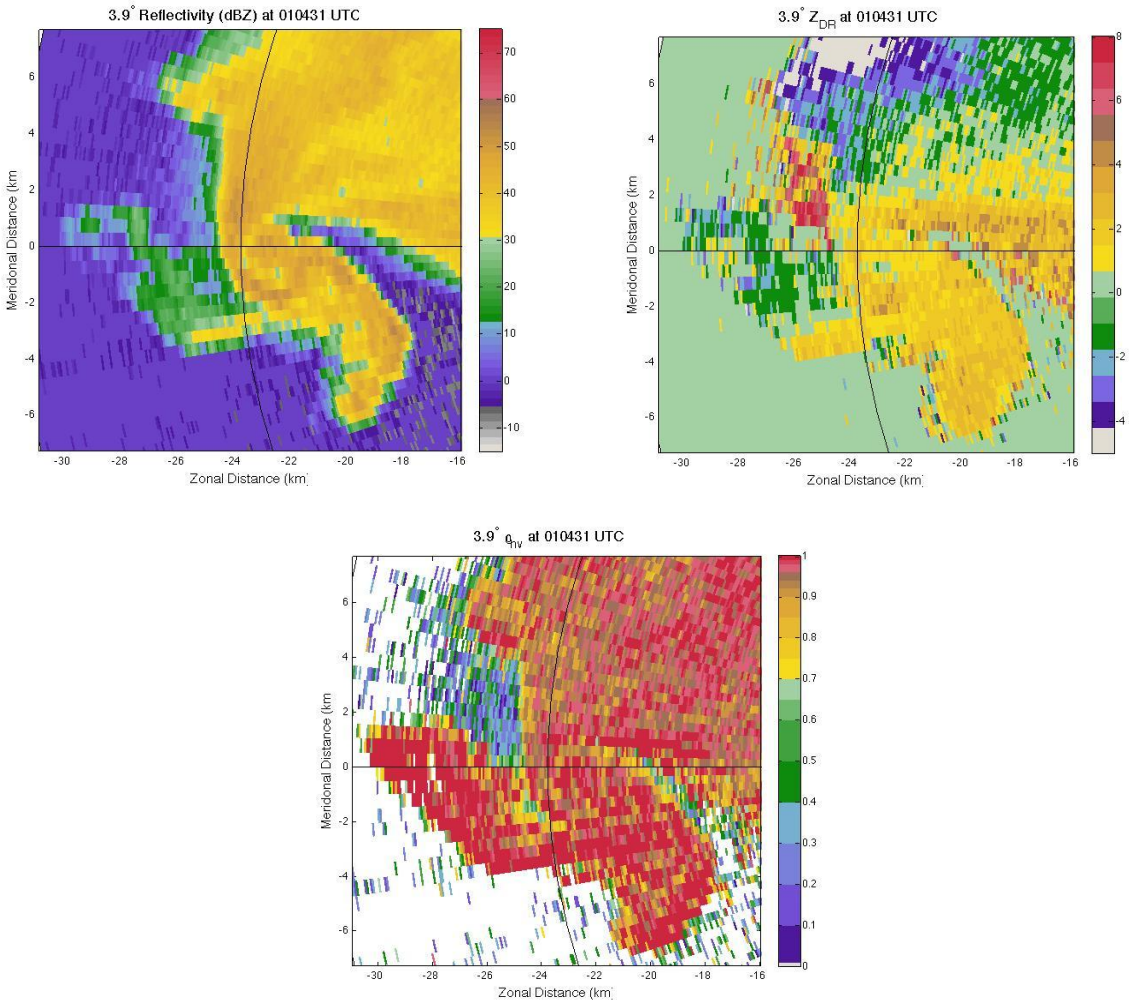

Figure 8: 3.9° scan showing Z, Z_{DR} and ρ_{hv} at 0104:30 UTC. Note the TBSS around x=-26, y=2.

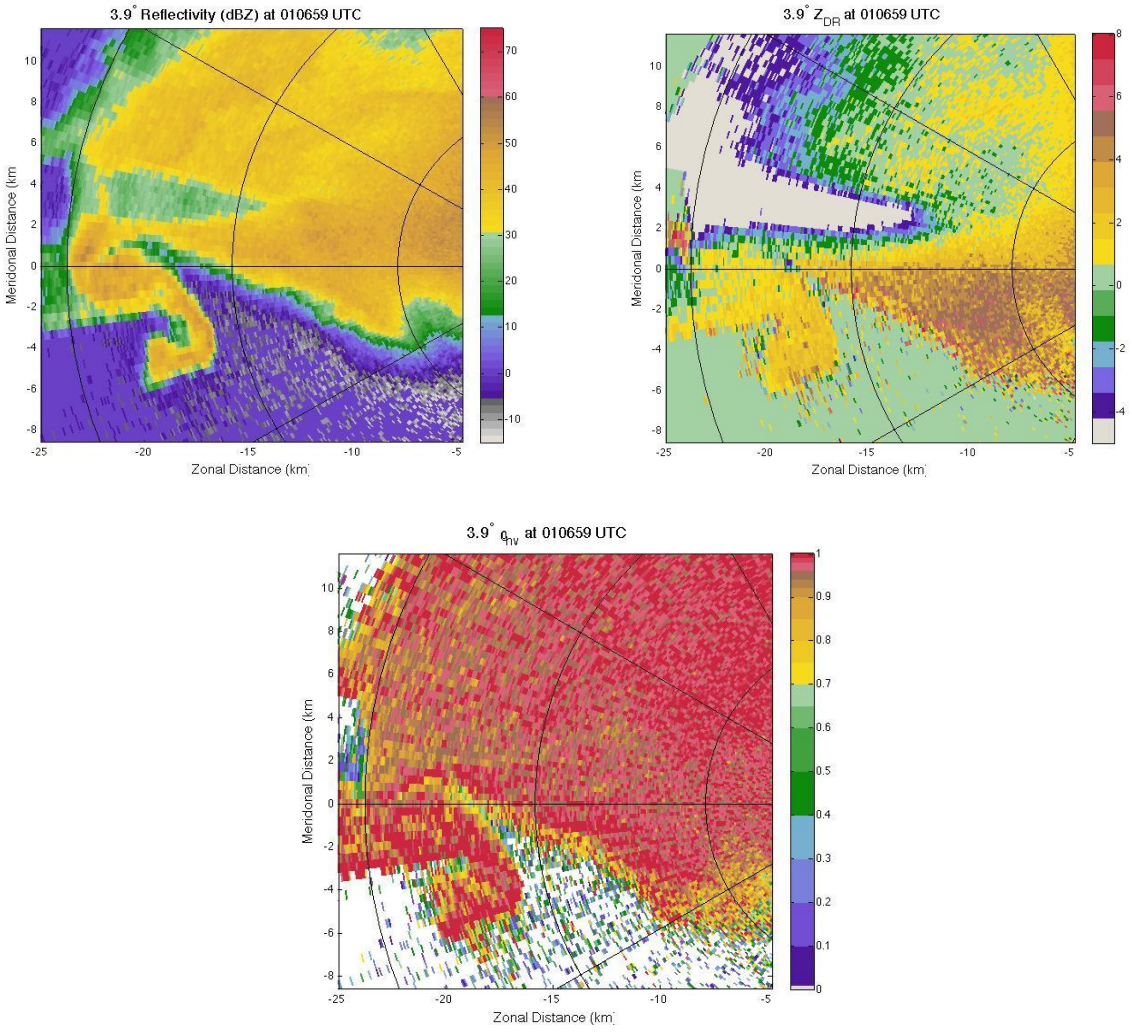

Figure 9: As in Figure 8, except for 0107 UTC. Note the attenuation in the Z and Z_{DR} fields. Also note the slightly lowered ρ_{hv} values where Z values remain high around x=-12, y=1.

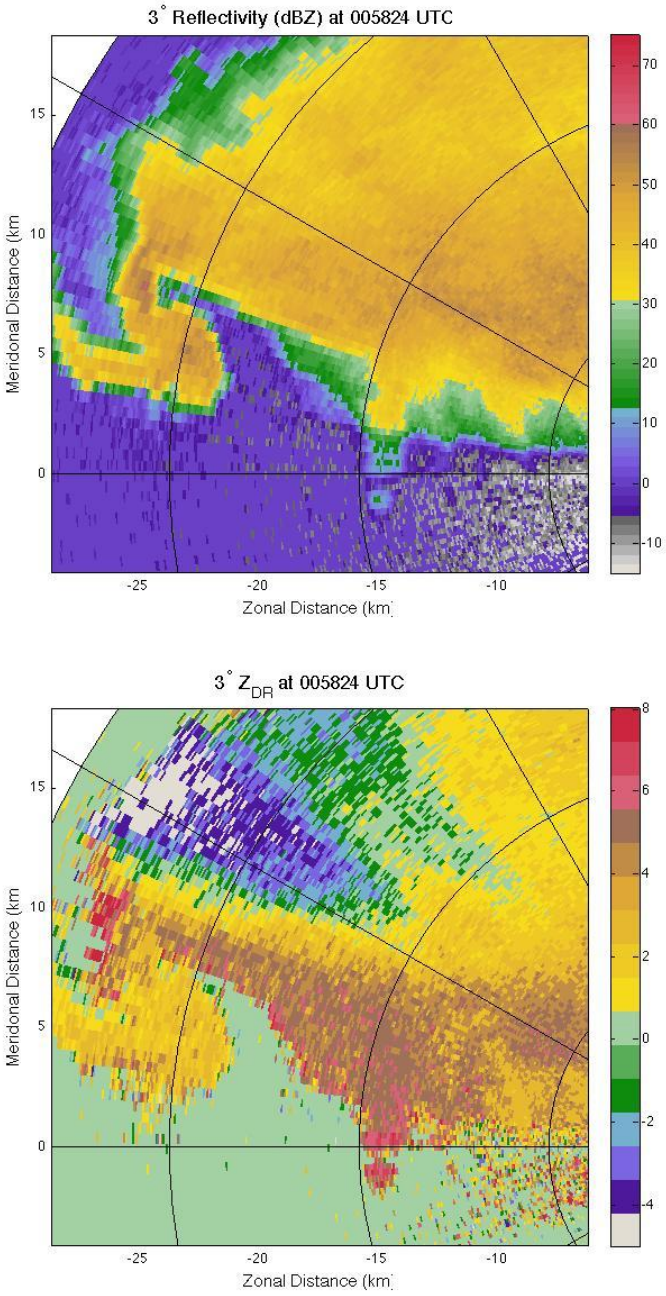

Figure 10: 3° scan showing Z and Z_{DR} at 0058:24 UTC.

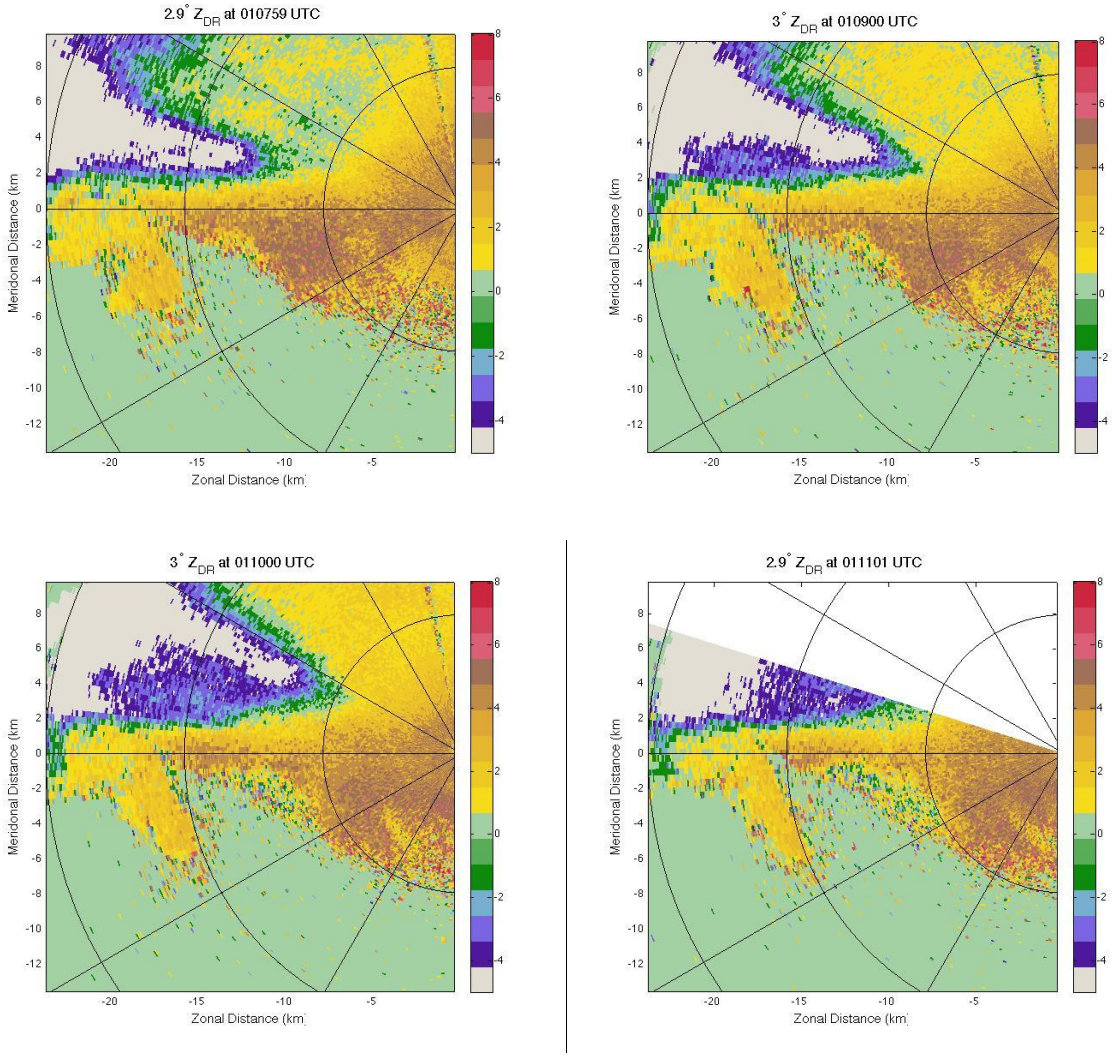

Figure 11: Time series of the 3° scan showing Z_{DR} at 0108, 0109, 0110 and 0111 UTC. The dissipation of the Z_{DR} arc is observed during this period.

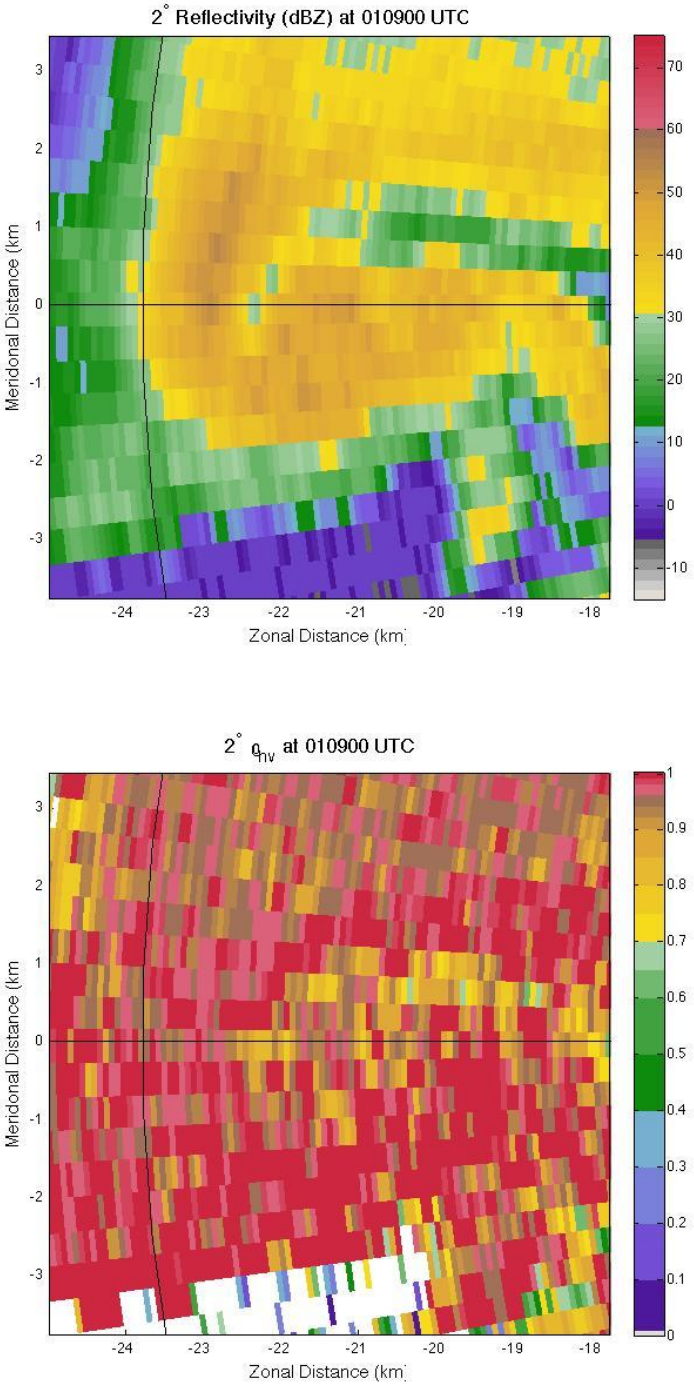

Figure 12: 2° scan showing Z and ρ_{hv} at 0109 UTC.

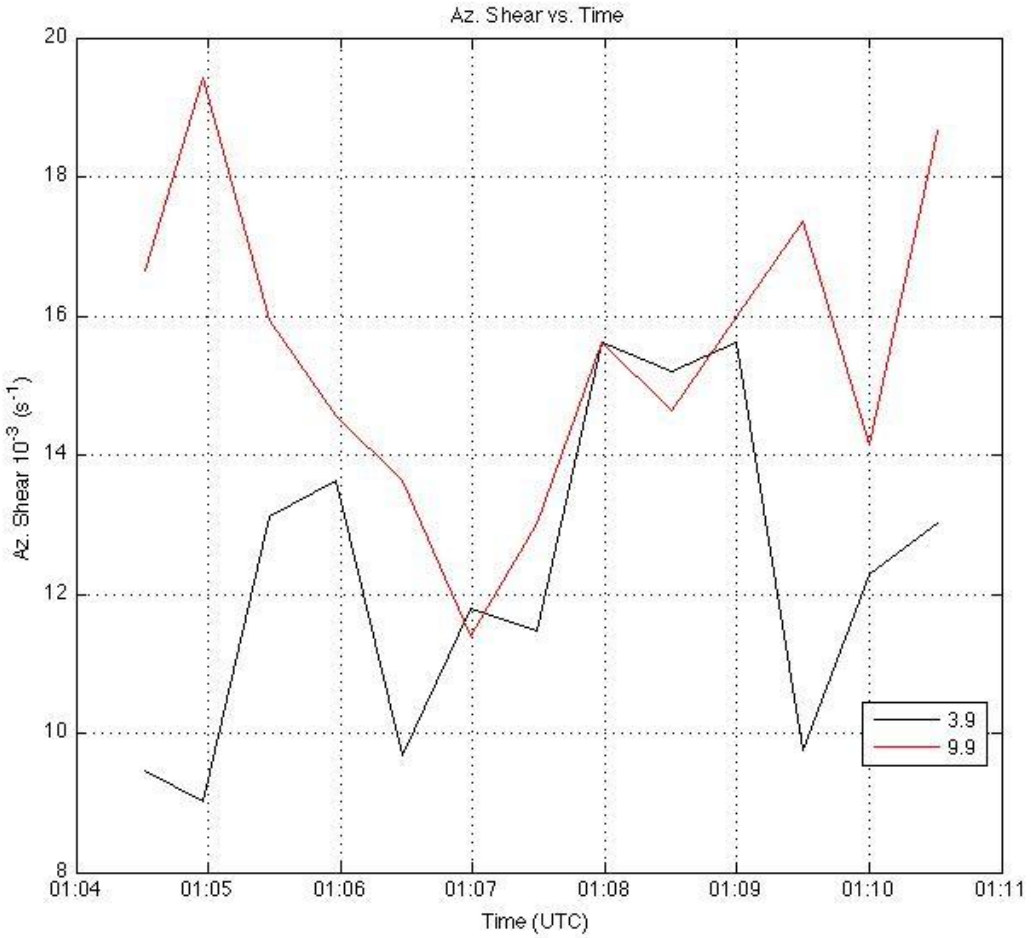

Figure 13: Azimuthal shear versus time from 0104:30 UTC to 0110:30 UTC for the 3.9° (black) and 9.9° (red) elevation scans.

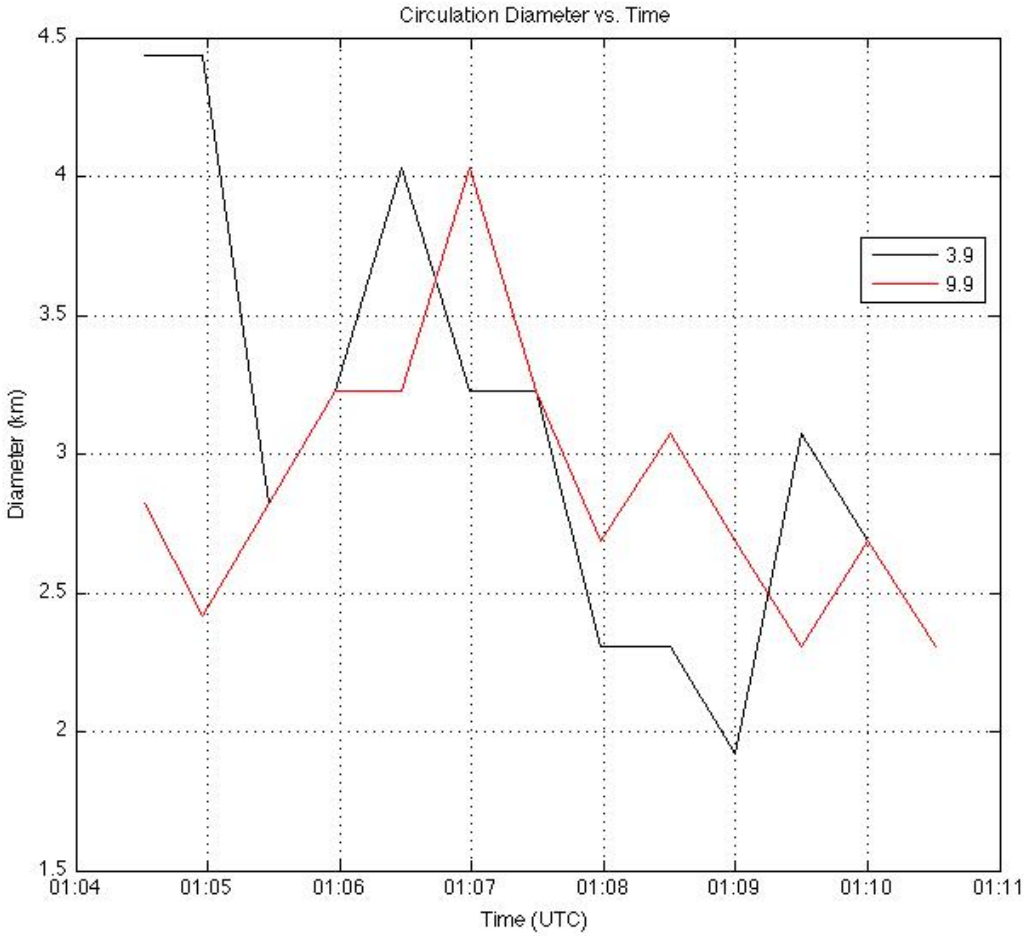

Figure 14: Change in circulation diameter versus time from 0104:30 UTC to 0110:30 UTC of the low-level mesocyclone (3.9°, black) and the midlevel mesocyclone (9.9°, red).

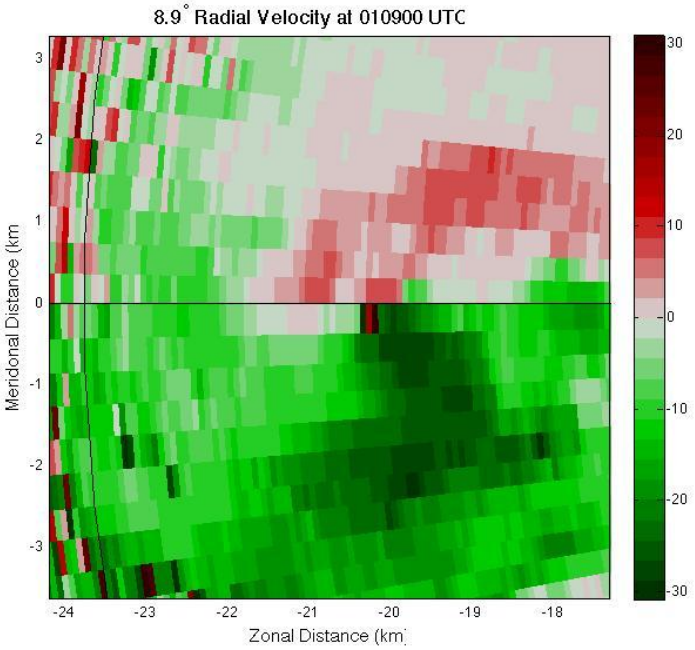

Figure 15: 8.9° scan of the Doppler velocity field at 0109 UTC.

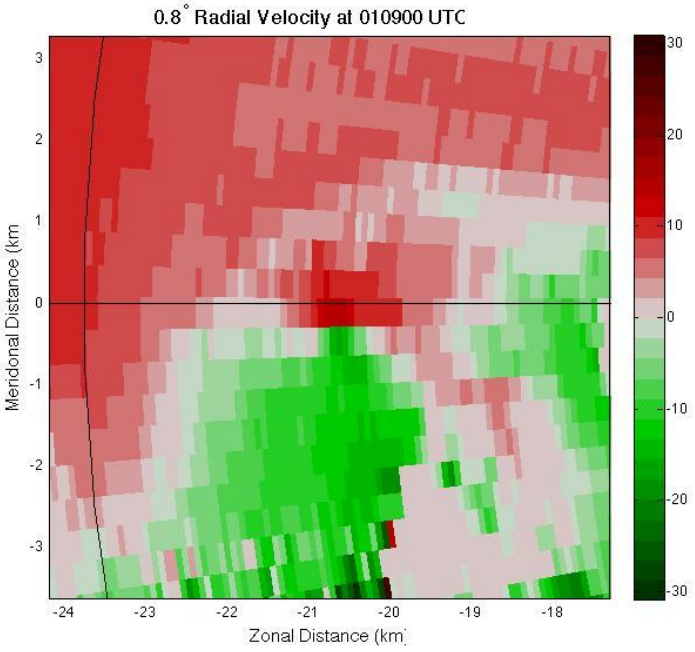

Figure 16: As in Figure 15, except for the 0.8° scan.

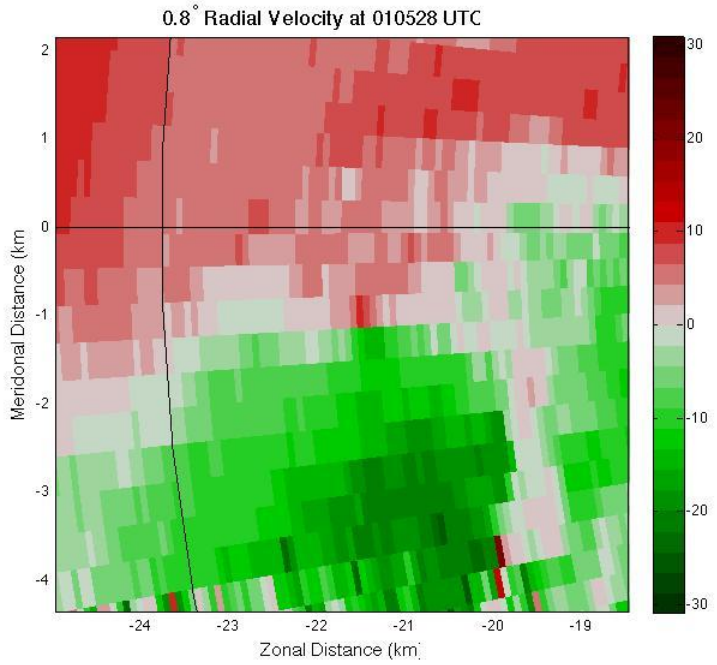

Figure 17: 0.8° scan of Doppler velocity at 0105:30 UTC.

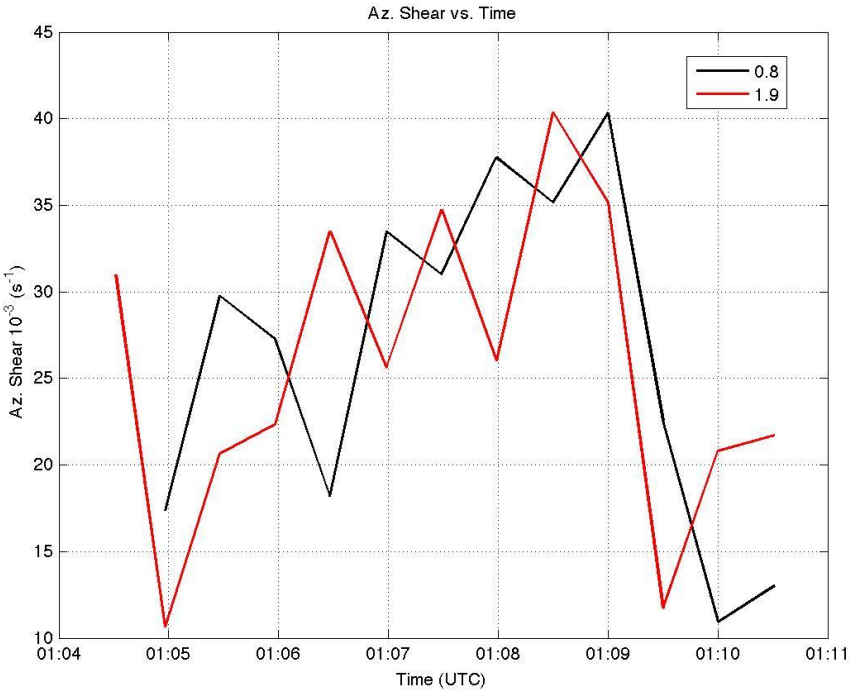

Figure 18: Change in azimuthal shear versus time of the 0.8° and 1.9° elevation scans. Note the increasing trend before a sharp drop after 0109 UTC.

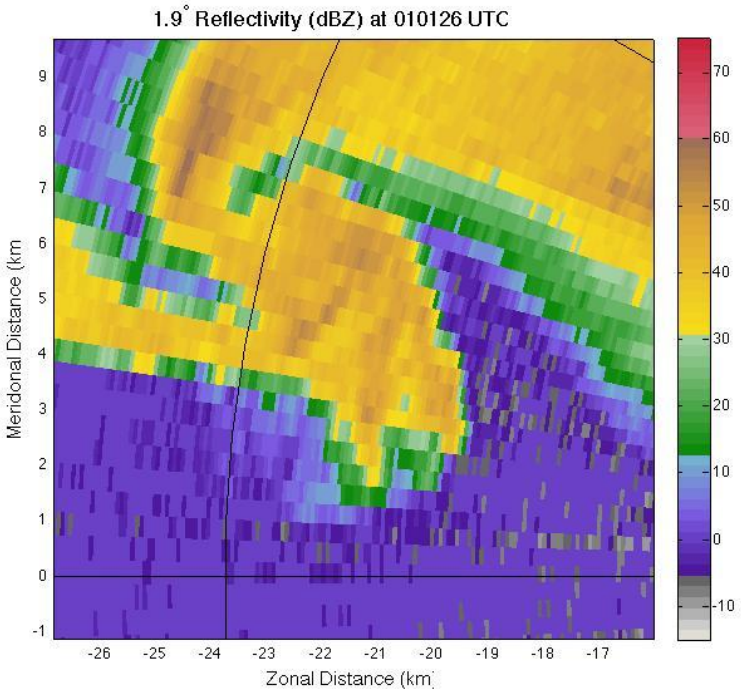

a)

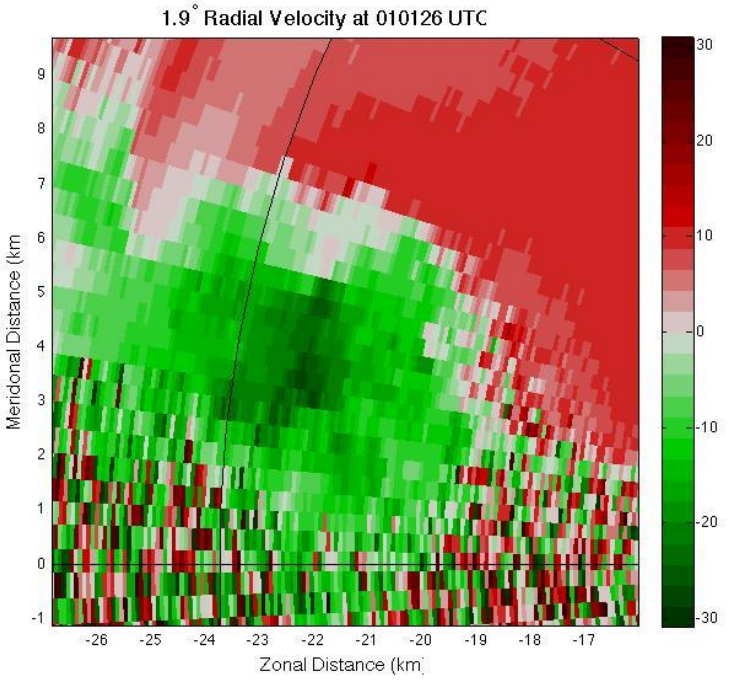

b)

Figure 19: 1.9° scan of the reflectivity field (a) and the velocity field (b) at 0101:30 UTC. Note the appendage in (a) at x =-21, y=2.

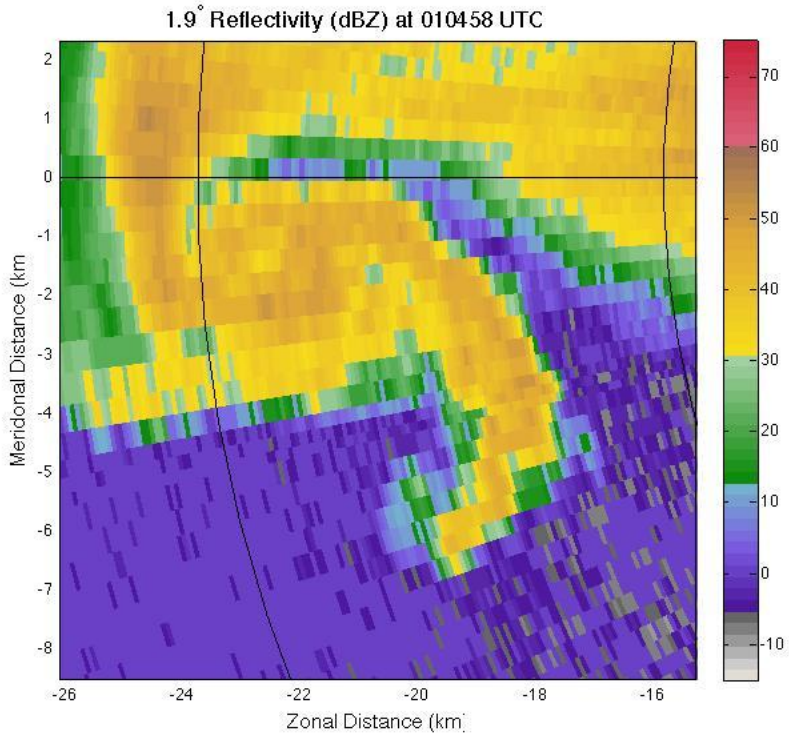

a)

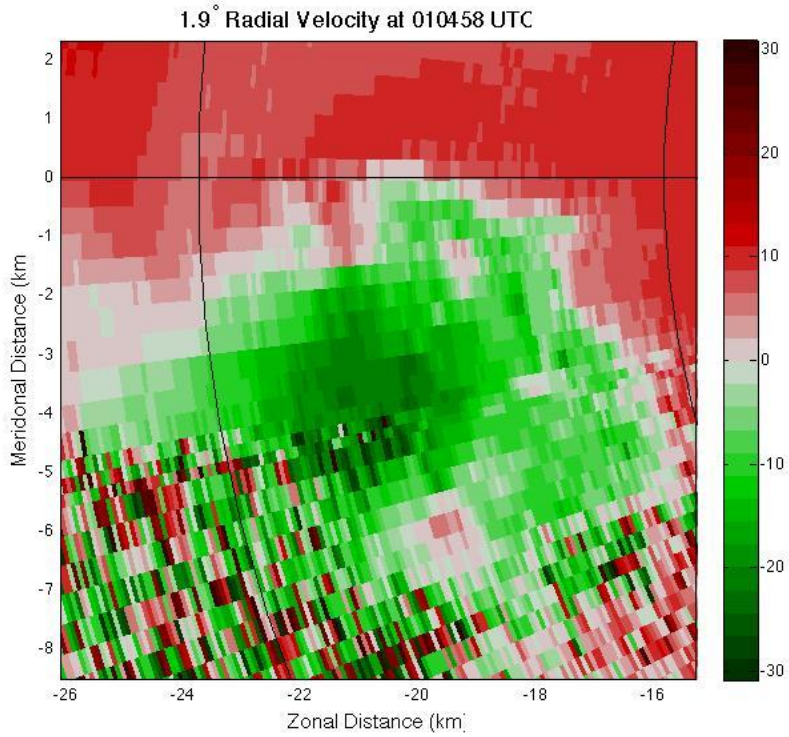

b)

Figure 20: 1.9° scan of the reflectivity field (a) and the velocity field (b) at 0105 UTC.

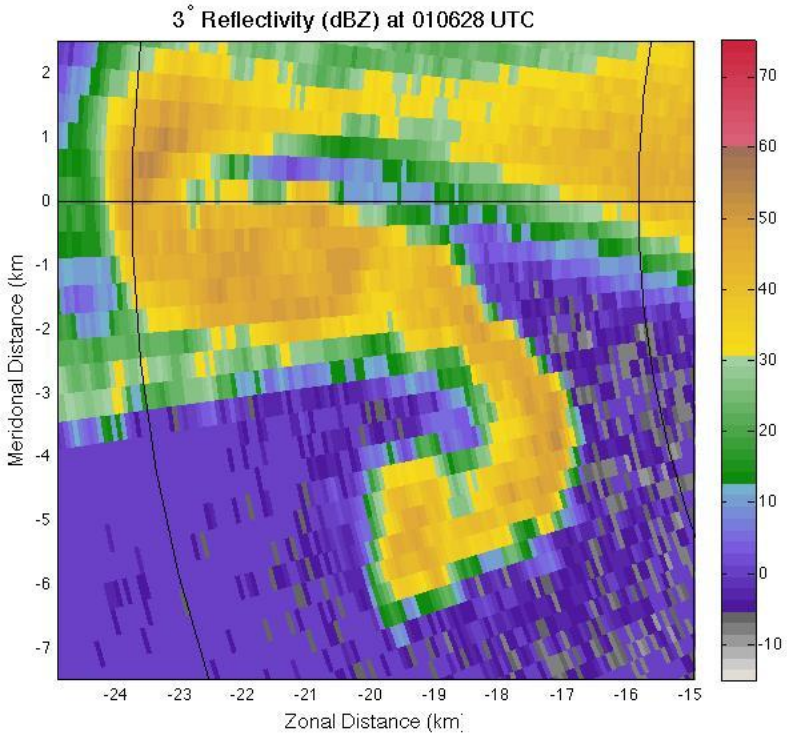

a)

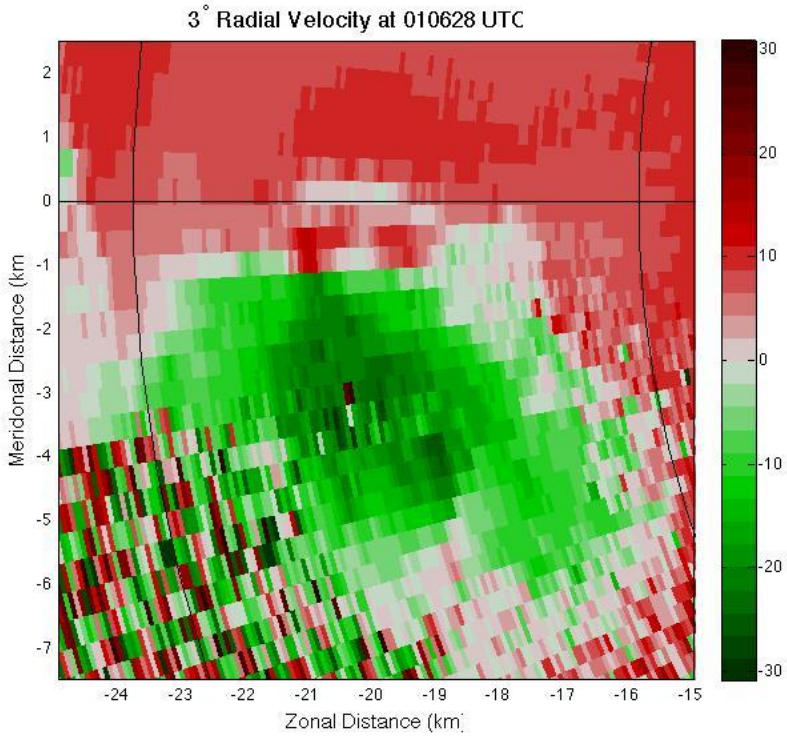

b)

Figure 21: As in Figure 20, except for 3° and at 0106:30 UTC.

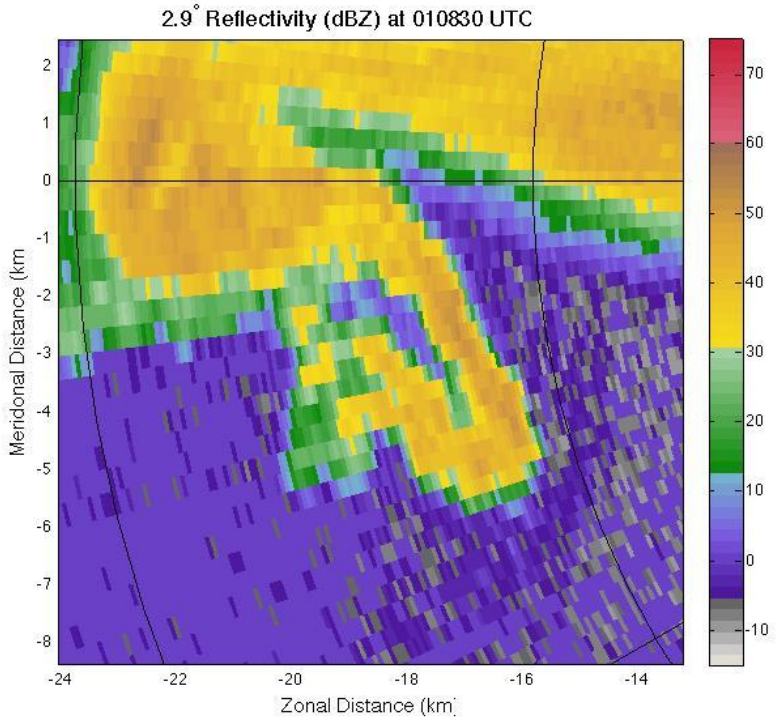

Figure 22: 2.9° scan showing Z at 0108:30 UTC.

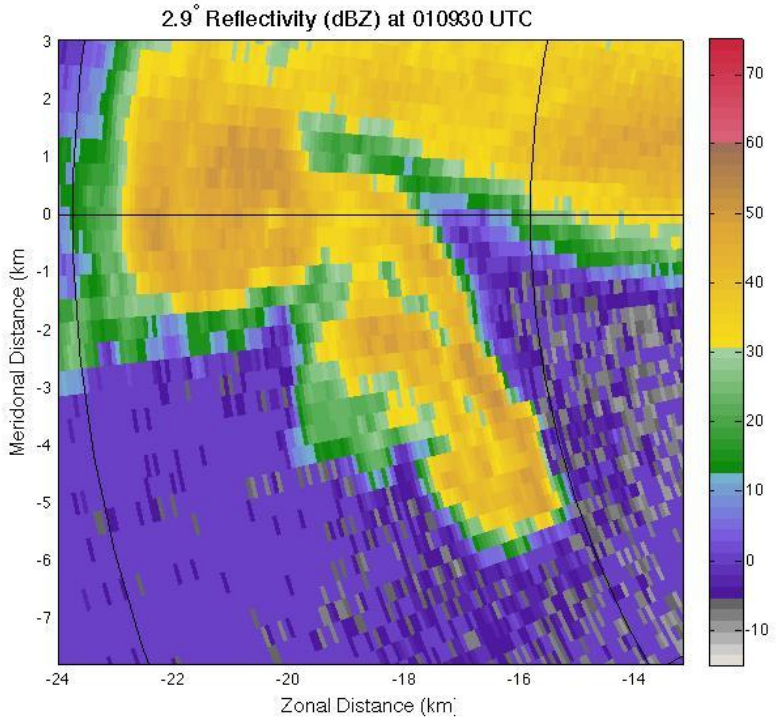

Figure 23: As in Figure 22, except for 0109:30 UTC.

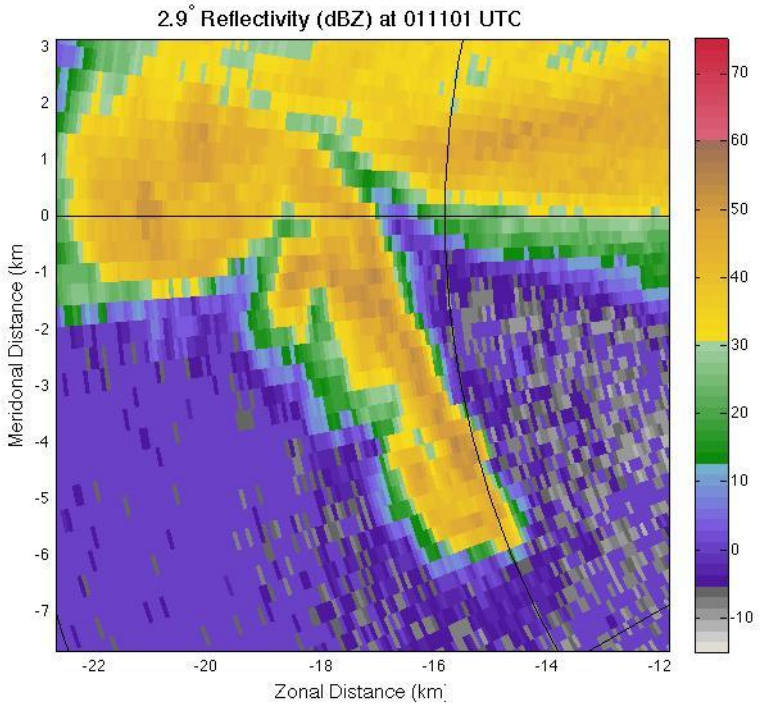

Figure 24: As in Figure 22, except for 0111 UTC.